

## Article

# Aridification in the Asian Interior Recorded by Mineral Assemblages in Tarim Basin since the Late Miocene and Its Link to Global Cooling

Maojie Yang<sup>1,2</sup>, Hong Chang<sup>1,3,\*</sup> , Xiuling Qin<sup>1,2</sup>, George S. Burr<sup>1</sup> and Weiguo Liu<sup>1,3</sup>

<sup>1</sup> State Key Laboratory of Loess and Quaternary Geology, Institute of Earth Environment, Chinese Academy of Sciences, Xi'an 710061, China

<sup>2</sup> University of Chinese Academy of Sciences, Beijing 100049, China

<sup>3</sup> CAS Center for Excellence in Quaternary Science and Global Change, Xi'an 710061, China

\* Correspondence: changh@loess.llqg.ac.cn; Tel.: +86-29-62336218

**Abstract:** Understanding climate change during the relatively warm Pliocene, as compared to the present, offers significant potential for understanding future global consequences of rising atmospheric CO<sub>2</sub>. Sensitivity differences among various climate proxies lead to divergent interpretations of the driving mechanisms of inland aridification. Minerals as a paleoclimatic indicator with high water-sensitivity can provide effective support for reconstructing climate evolution and clearly understanding driving mechanisms in extremely arid regions. Here we present results of mineral analyses from lacustrine–fluvial Neogene sediments in the eastern Tarim Basin. Evaporite minerals are composed principally of calcite, dolomite, and gypsum, with minor amounts of ankerite and celestite. Clay minerals are dominated by illite and chlorite. We find that evaporite minerals and illite reflect regional climate change through time, and specifically determine the following: (1) climate in the Tarim Basin during the late Miocene was relatively humid, with alternating dry and wet periods from 6.86–5.58 Ma; (2) immediately following that interval, aridification increased rapidly, with reduced regional precipitation that accelerated the shrinkage of the lake; (3) from 4.4 Ma to 3.62 Ma, regional precipitation increased slightly but afterwards, aridification resumed: the climate there has been extremely dry since about 2.7 Ma. Our results show that the climate in the Tarim Basin has followed a global cooling trend since the late Miocene, and suggest that the effect of uplift in the Tibetan Plateau is a secondary influence.

**Keywords:** minerals; Tarim Basin; westerly wind; global cooling; Asian interior aridification; late cenozoic



**Citation:** Yang, M.; Chang, H.; Qin, X.; Burr, G.S.; Liu, W. Aridification in the Asian Interior Recorded by Mineral Assemblages in Tarim Basin since the Late Miocene and Its Link to Global Cooling. *Minerals* **2022**, *12*, 1543. <https://doi.org/10.3390/min12121543>

Academic Editor: János Haas

Received: 1 November 2022

Accepted: 24 November 2022

Published: 30 November 2022

**Publisher's Note:** MDPI stays neutral with regard to jurisdictional claims in published maps and institutional affiliations.



**Copyright:** © 2022 by the authors. Licensee MDPI, Basel, Switzerland. This article is an open access article distributed under the terms and conditions of the Creative Commons Attribution (CC BY) license (<https://creativecommons.org/licenses/by/4.0/>).

## 1. Introduction

The climate of the Asian interior is mainly controlled by the westerlies. Details of climatic deterioration in this extremely arid region since the late Miocene have been derived from a variety of climate indicators [1–3], and differences in the sensitivity and fidelity between them have led to some controversy over the driving mechanisms of inland aridification [4,5]. Taking the Tarim Basin as an example, soluble salts preserved in lacustrine–deltaic sediments from the western basin [6] and oxygen isotope records from sediments in the eastern basin [7] suggest relatively humid conditions during the early Pliocene. In contrast, pollen records from the northern basin [8] and biogenic Ba records from lacustrine sediments from the eastern basin [9] indicate enhanced aridity in the same interval. Two possible climatic drivers, proposed by the above climate indicators, may have triggered the enhanced aridification: (1) tectonic uplift of the Tibetan Plateau, or (2) global cooling [10,11]. To estimate the relative contribution from these two factors, a paleoclimate proxy that is sensitive to aridification is needed.

Minerals found in all surface sediments and sedimentary rocks are particularly sensitive to precipitation variations in arid regions [12,13]. They are faithful carriers of paleoclimatic signals [14]. Evaporite minerals (carbonates and sulfates) and clay minerals are among the most common minerals found in marine and lacustrine sediments [15–17]. Carbonates and sulfates are chemical products that are especially sensitive to the degree of aridity, while clay minerals are products of rock chemical weathering. Authigenic evaporite minerals form in saline lakes and reflect sedimentary environmental conditions where they crystallize [18,19]. Clay minerals respond to regional humidity changes under stable tectonic conditions [20]. To trace the aridification of the Asian interior through time and determine its driving mechanisms, we investigated evaporites and clay minerals from a Cenozoic lacustrine–fluvial sequence (drill core Ls2) in the Tarim Basin ( $39^{\circ}47' \text{ N}$ ,  $88^{\circ}23' \text{ E}$ ), north of the Tibetan Plateau (Figure 1). As minerals have high water-sensitivity, high-resolution paleoclimate variations deciphered with mineralogy allow for a better understanding of past climate change, particularly with regard to the major effects that global cooling had on the Asian interior aridification.

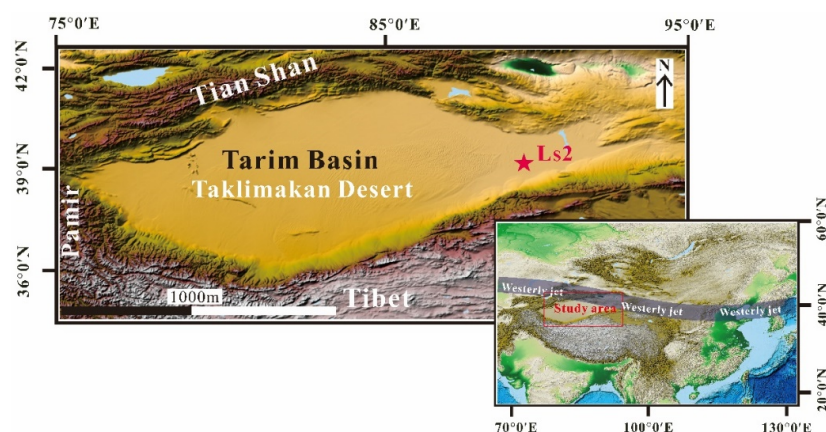


**Figure 1.** Location map of drill core Ls2 and the westerly jet.

## 2. Methods

The mineral measurements were carried out for samples from drill core Ls2 in the eastern Tarim Basin (Figure 1), covering a depth of 1003.92 m and going back to  $\sim 6.865 \text{ Ma}$  [21]. Samples were taken at  $\sim 5 \text{ m}$  interval, and a total of 183 samples were taken for mineral analysis. Bulk samples were ground, and 1.8 g of powdered sample mixed with 9 g of inlay, which consisted of epoxy resin and coagulant with a mass ratio of 25:7. The homogeneous mixture was made and then evacuated and sonicated until all air bubbles were eliminated. After the mixture cured, its surface was ground and polished to obtain standard mineral specimens.

The standard mineral specimens were scanned using a ZEISS EVO 18 scanning electron microscope (SEM) with energy-dispersive spectroscopy (EDS) and controlled by an advanced mineral identification and characterization system (AMICS) to identify the mineral composition. Due to the high analysis speed and test accuracy of the AMICS, different characteristic mineral parameters can be automatically analyzed and quantified. All sample analyses were carried out using a 20 kV acceleration voltage and a probe current of 1 nA. The number of mineral particles analyzed per sample was about 3000–4000 grains. Additionally, the powdered samples were scanned using SEM-EDS to determine their mineral morphology characterization. The above-mentioned analyses were conducted at the Institute of Earth Environment for the Chinese Academy of Sciences.

## 3. Results

### 3.1. Carbonates

Carbonate minerals in samples from drill core Ls2 include calcite, dolomite and ankerite (Figure 2, supplementary). Dolomite is the major carbonate phase present through-

out the profile. Its morphology is spheroidal (Figure 3), and dolomite content ranged from 0~8.46% and decreased significantly above a depth of 673.52 m (4.92 Ma). This suggests a persistent change in chemical conditions in the paleolake since that time. Spheroidal ankerite abundance ranges from 0~7.46%, centered mainly at 942.91~938.21 m (6.43~6.40 Ma), 913.22~888.69 m (6.26~6.17 Ma), and 814.7 m depth (5.8 Ma). The ankerite content in the other layers is less than 1%. Dolomite content decreased dramatically during stages with high ankerite contents. Calcite (0~5.02%) is the next most abundant carbonate, and increased gradually upward in the section. Most calcite exhibits a dense granular and flaked morphology (Figure 3).

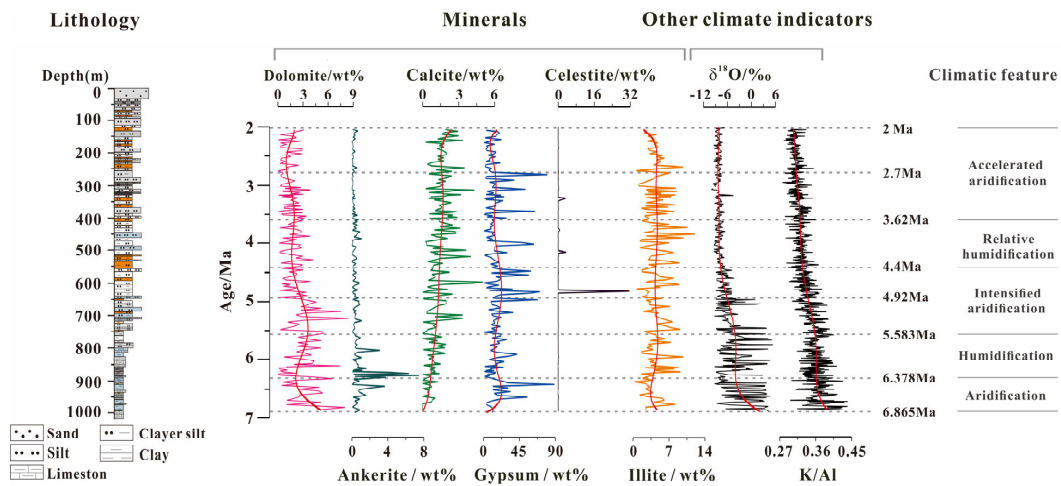


Figure 2. Lithological profiles [21], minerals (this study),  $\delta^{18}\text{O}$  [7] and K/Al [5] in lacustrine sediments from drill core Ls2 in the eastern Tarim Basin. Red curves represent long-term trends.

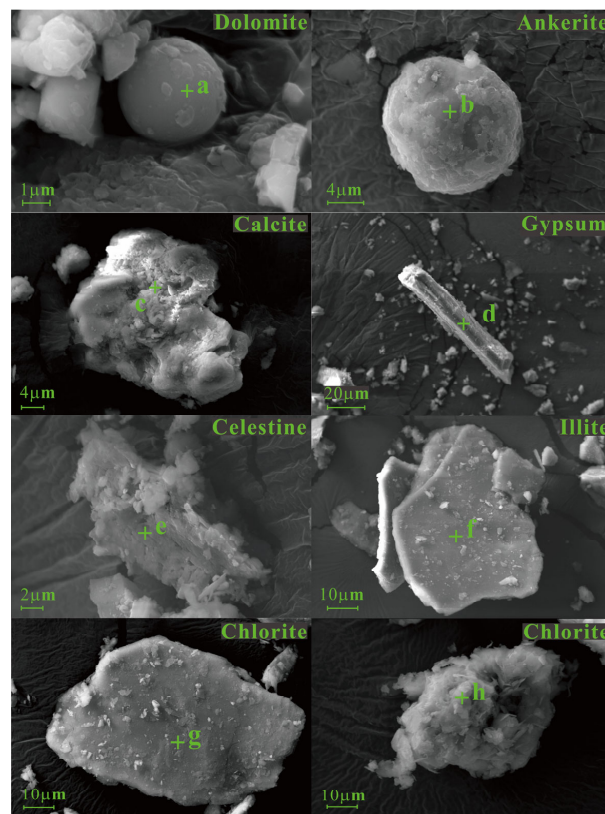


Figure 3. Microscopic morphology of carbonates, sulfates and clay minerals in drill core Ls2. Spheroidal dolomite (a) and ankerite (b), dense granular and flaked calcite (c), columnar gypsum granular (d), celestite aggregate (e), plate-shaped illite (f) and chlorite (g), and flower-like chlorite (h).

### 3.2. Sulfates

As shown in Figure 2, sulfate occurrence in the core is discontinuous. Relatively high amounts of gypsum appear at 1003.92~923.17 m (6.865~6.317 Ma), 673.52~496.25 m (4.92~3.94 Ma), 389.67~384.97 m (3.39~3.37 Ma) and 289.45~251.72 m depth (3.01~2.76 Ma). The gypsum content in the other layers does not exceed 10%. Celestite content in most samples is less than 0.3%, except at 652.71 m (4.8 Ma), 530.08 m (4.14 Ma), and 361.12 m depth (3.21 Ma), which contain 31.62%, 3.58% and 3.41% celestite, respectively. The edges and corners of columnar gypsum and granular celestite aggregates (Figure 3) are relatively complete without obvious wear scars, which suggests that these mineral particles were not transported.

### 3.3. Clay Minerals

Plentiful plate-shaped illites and chlorites, accompanied by a small amount of flower-like chlorite, are observed in the site (Figure 3). The illite content is relatively high (0.25%~12.06%) as compared to chlorite (0.14%~3.45%), and its content fluctuates greatly below 673.52 m (4.92 Ma). Illite content increases at 673.52~486.47 m depth (4.92~3.88 Ma), and then remains relatively constant at 486.47~246.67 m depth (3.88~2.7 Ma). After that, a decreasing trend is observed.

## 4. Discussion

### 4.1. The Paleoclimatic Significance of Minerals

#### 4.1.1. Carbonates

In arid regions, soluble salts from areas surrounding lakes accumulate with time through surface runoff. If evaporation is greater than precipitation in a catchment, chemical deposition in lakes is dominated by the precipitation of evaporated salts [22]. Carbonates will gradually precipitate out of the lake when it is in a supersaturated state [23]. Hydrochemical parameters (e.g., Mg/Ca, pH, etc.) are controlled by the amount of regional precipitation [24,25]. The arid climate will promote the continuous shrinkage of the lake to precipitate a large amount of calcite. In addition, both strong evaporation and mediation by microorganisms (sulfate-reducing bacteria) can induce spheroidal dolomite formation (Figure 3) [26]. Spheroidal ankerite is formed when more than half of the magnesium ions in the dolomite lattice are replaced by iron. A possible iron source for ankerite formation is derived from the breakdown of detrital Fe-Mg minerals during deposition. Microbial mediation may be a dominant factor for dolomite/ankerite precipitation in a depositional environment, with increasing long-term evaporation [26,27]. A decrease in lake level may limit microbial activity, as it is not conducive to dolomite/ankerite deposition. Therefore, calcite may be favored in shrinking lakes, while dolomite/ankerite can precipitate in relatively stable lakes.

#### 4.1.2. Sulfates

Layered gypsum crystals form in the lake when a sharp drop in surface supplemental runoff occurs and salinity rises [28]. Celestite is a typical indicator mineral of an arid and high evaporation environment, and its presence suggests dry conditions in and around the lake. As rocks and minerals, exposed at the earth's surface, come into contact with surface water, soluble chemical elements such as Sr are brought by surface water to low-lying areas, where they accumulate [29]. A progressively drier climate causes  $\text{Sr}^{2+}$  to become concentrated in closed lake basins and promotes celestite precipitation in the lakes.

#### 4.1.3. Clay Minerals

Clay minerals in sediments are sensitive to climatic conditions and weathering intensity [20,30]. Illite can be preserved under strong physical weathering conditions [31]. Sediment diagenesis also influences clay mineral compositions [32], e.g., the transformations of smectite to illite that occur under alkaline pore water conditions with increasing burial depth. Under the influence of diagenesis, mixed-layer minerals (e.g., I/S) are prone

to appear in the transformation process between clay minerals [33,34]. Clay minerals cannot be directly used as a climate indicator when mixed-layer minerals are found in sediments [35,36]. In drill core Ls2, only illite and chlorite are present, and most of them are plate-shaped (Figure 3), which indicates that most of the clay minerals are exogenous. Small amounts of flower-like chlorite, however, are observed in some sections (Figure 3), and may be directly transformed from other clay minerals eroded by Mg/Fe-rich fluids [37]. Thus, chlorite content cannot be used to reconstruct paleoclimates because of its complex origin and erosion after deposition [38]. Therefore, we employ illite in drill core Ls2 to trace climate change.

In general, illite, also known as hydromica, is usually formed by the weathering of aluminosilicate minerals, such as feldspar and mica, in cold and dry climates [17]. Its existence represents a typical cold and arid climate, because it is unstable and easily decomposes under acidic conditions. Nevertheless, illite may also indicate weak chemical weathering in the absence of montmorillonite and kaolinite. Slight increases in regional precipitation can facilitate the weathering–leaching of feldspar and mica, and lead to the formation of illite. Based on this inference, clay minerals offer a means to understand weathering histories and past climates.

#### 4.2. Implications for Climatic Change

Our paleoclimatic reconstruction is based mainly on mineral assemblages from Lop Nor. As climate changed in the eastern Tarim Basin, lake water rose and then retreated; and carbonates, sulfates and illite were affected. The mineral data below are compared with  $\delta^{18}\text{O}$  records [7] that reflect precipitation and K/Al [5] as a measure of chemical weathering in the Ls2 drill core. Paleoclimate fluctuations at the site can be divided into 5 phases as follows (Figure 2):

##### 1. Aridification (6.865~6.378 Ma)

Mineral data suggest a gradual rise in lake water pH between 6.865~6.378 Ma, as the proportion of ankerite rose and dolomite decreased [30,39]. Gypsum and calcite also increased at this time, pointing to increased evaporation in the catchment area. Low clay content in the lower part of the core implies strong physical denudation or/and reduced chemical weathering. Taken together, these features indicate significant aridification during this stage. Pollen evidence support this view, with expansion of Xerophytic taxa in Northwest China at the time [40].

##### 2. Humidification (6.378~5.583 Ma)

This climate phase was more humid as judged by an increase in illite. A possible higher river discharge facilitated the transport of relatively soluble ions from the catchment rocks into the lake. A deep and stable lacustrine sedimentary environment with high lake productivity was also favorable for carbonate deposition [41]. The reason why ankerite concentrated in the early stage (6.257~6.169 Ma) of this phase was probably there was a relatively high porosity of dolomite, which facilitated  $\text{Fe}^{3+}$  enrichment, and microbially mediated ankerite deposition [27]. Reduced evaporation resulted in a decreased gypsum content, which consistent with the comparatively low soluble salt content observed during 5.9~5.6 Ma in the northern and southern Tarim Basin [42,43].

##### 3. Intensified aridification (5.583~4.4 Ma)

A dry event that began at 5.583 Ma is well documented by mineral assemblages. Increased aridity inhibited chemical weathering and thus decreased the proportion of illite at this time. Due to reduced humidity in the region, the amount of water replenished by precipitation was insufficient to compensate for evaporative losses. So, the lake level fell and salts accumulated in the lake basin, with increased gypsum and calcite contents. The decrease in dolomite content since 4.92 Ma was likely associated with a strong drop in lake level, or a transition from a lacustrine to fluvial environment (Figure 2). Shrinkage of the lake would eliminate the anaerobic environment which was necessary for microbially

mediated chemical reactions. Another indicator of very dry conditions is the large amount of celestite precipitated at 4.8 Ma, possibly from the late stage of a permanent lake in the study area [32]. Drought conditions persisted until 4.4 Ma.

#### 4. Relative humidification (4.4~3.62 Ma)

Mineralogical changes from 4.4~3.62 Ma were similar those seen in the period between 6.378 Ma and 5.583 Ma, indicating a rise in regional precipitation. Humidification from the same period is recorded by sediments in the Kuchetawu section in the southern foreland basin of the Tianshan Mountains [43], a phenomenon accompanied by a period of increased chemical weathering (Figure 4). Our results are also consistent with a climatic record of a late Cenozoic succession in the central Taklimakan Desert, where fine bedding with deep red color indicates the presence of surface water during 4.2~3.4 Ma [44].

#### 5. Accelerated aridification (3.62~2 Ma)

The early Pliocene increase in relative humidification was followed by a late-Pliocene aridity event that began at about 3.62 Ma, accompanied by further shrinkage of lakes [6] and rapidly expanding deserts [45] in the Tarim Basin. The apparent increase in gypsum content at this time indicates a decrease in regional humidity. The aeolian flux in the southern margin of the Taklimakan Desert increased sharply at 3.6 Ma (Figure 4), suggesting increased aridity, and the intensity of westerly winds increased significantly in the late Pliocene [46]. Large-scale aeolian dunes dominated the paleoenvironment of the basin since ~2.7 Ma [3]. Weak chemical weathering and reduced surface runoff limited clay formation and transport into the catchment, while high evaporation facilitated carbonate precipitation from supersaturated brines. All in all, the climate continued to be extremely arid in the Tarim Basin during the period of 3.62~2 Ma.

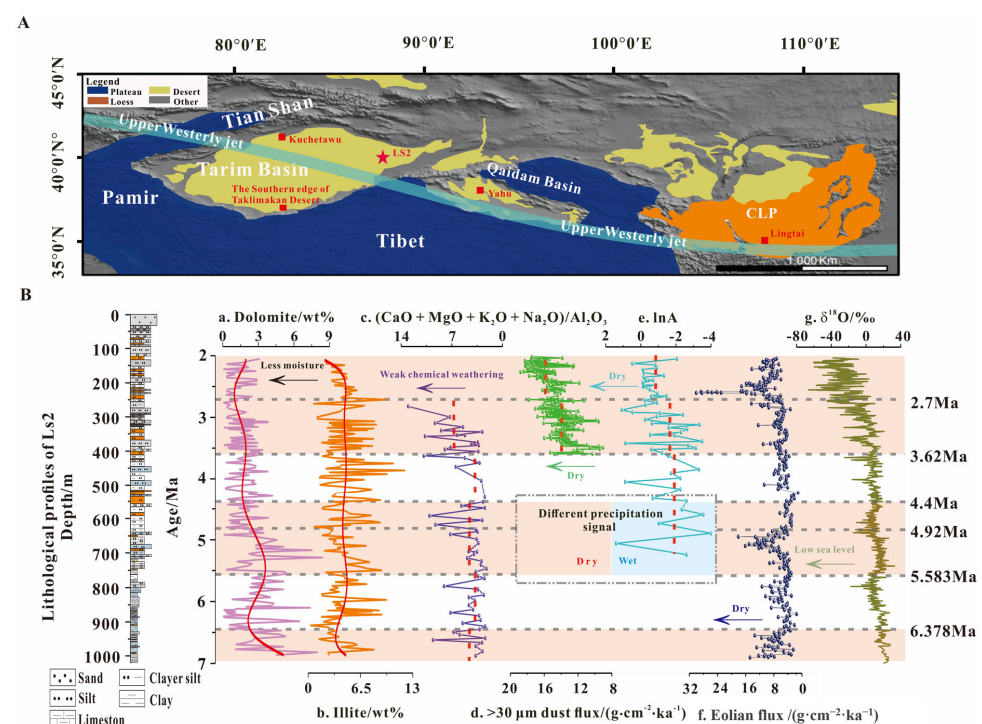


**Figure 4.** Comparison of climatic indices from different areas. (A) Map of different areas in the Asian interior, where climate is dominated by the westerlies (Modified from [47]) (B) Correlation of minerals from drill core Ls2 in the eastern Tarim Basin (a, b: this study) with (c) weathering index  $(\text{CaO} + \text{MgO} + \text{K}_2\text{O} + \text{Na}_2\text{O})/\text{Al}_2\text{O}_3$  from the Kuchetawu section, northern Tarim Basin [8], (d)  $>30 \mu\text{m}$  grain size of eolian flux in the loess core from southern margin of the Tarim basin [46], (e) aridity index  $\ln A$  from the Yahu section in the Qaidam basin [48], (f) eolian flux from the Lingtai section, Chinese Loess Plateau [49], and (g) global deep-sea oxygen isotopes. The red area and the blue area represent intervals of relatively arid and humid climate, respectively.

#### 4.3. Late Cenozoic Westerlies Evolution Drove by Global Cooling

Sustained late Cenozoic global cooling could have contributed to environmental changes in the Asian interior by reducing the intensity of the global hydrological cycle. Comparisons of different regional climatic records in northwest China (Figure 4B) reveal prevailing arid conditions in the Asian interior since the late Miocene [43,50]. Based on the coupling between global deep-sea oxygen isotopes [51] with eolian fluxes in the Asian interior [49] and regional climate events, we argue that the evolution of the westerlies, driven by global cooling, controlled the overall precipitation in the Tarim Basin. For instance, the intensification of aridification observed at 5.583 Ma was also seen in the central Qaidam Basin since 5.3 Ma with the sporopollen-based climatic indicator (lnA) [52,53]. Dust-borne wind accumulation in the Lingtai profile in the Chinese Loess Plateau also provides evidence for a synchronous intensification of aridity [1,3]. These concurrent changes, during a time of global ice volume expansion, especially in Greenland [54], imply a reduction in westerly water vapor to the basin during the late Miocene–early Pliocene. Arid conditions in the Tarim Basin prevailed between 5.583 Ma to 4.4 Ma, while the climate in the Qaidam Basin seems to have been less dry [48,55]. Although some observations attribute the significant difference in precipitation in the northeastern Tibetan Plateau during the late Miocene–early Pliocene to an enhanced rain shadow caused by tectonic uplift of the Tibetan Plateau [53]; geochemical [8] and mineral (this study) indicators suggest that global cooling was the dominant factor in the Tarim basin. The regional climate responded to a reduction in moisture availability, which was in part due to moisture transport, even if the effects of the uplift of the Tibetan Plateau cannot be ruled out.

The spatial heterogeneity of precipitation in the regions mentioned above was likely influenced by a southward shift in the westerly jet stream, related to the expansion of the Arctic ice sheet [56]. The southward migration of the westerly winds reduced the amount of moisture that could reach the Tarim Basin, while the Qaidam Basin, located to the southeast, received more precipitation [48]. This inference provides a plausible explanation for the covariation of precipitation in the Tarim basin with glaciers in southeast Greenland [57] during 6.865–4.92 Ma. The westerly jet likely reached the northern Tibetan Plateau before 4.92 Ma. This change made it appear that climate change in the Tarim basin was mainly due to the rain shadow effect of the Tibetan Plateau [7,43]. Our results show, however, that evidence of warm and humid conditions [58,59] in the Pliocene were preserved in the Tarim Basin when the global atmospheric CO<sub>2</sub> content was higher. Specifically, increased water vapor carried by the westerly winds increased precipitation in the Tarim Basin from 4.4–3.62 Ma. Aridification in the Tarim Basin occurred, along with global ice expansion at 3.62 Ma, followed by rapid aridification after 2.7 Ma. As a result of reduced evaporation at the sea surface, owing to global cooling, the moisture supply to the Asian interior fell [60], and this further facilitated desertification. This consequence is consistent with an abrupt increase in aeolian dust flux in the Asian interior [49]. The southward migration of westerly winds may have brought moisture south of the basin, creating environments such as the Keriya valley on the northern edge of the West Kunlun Mountains, which experienced seasonal flooding, and wider rivers in the early Pleistocene as compared to the present [61].

Systematic mineral climatic indices provide a consistent picture of climate change in the Tarim Basin since the late Miocene and emphasize the role of the westerly winds. Our results show that global cooling was the dominant mechanism aridification in the Asian interior since the late Miocene [7,21].

## 5. Conclusions

Lacustrine deposits in the eastern Tarim Basin contain mineral records of aridification across the Asian interior through time. On the basis of an analysis of mineral content, several conclusions can be drawn, as follows:

Minerals can be used as sensitive climate indices to reconstruct the paleoclimate in the Tarim Basin since the late Miocene. Evaporites and illite, analyzed in a drill core sequence, show an oscillating pattern covering five distinct climate stages during the last 6.838 Ma.

Three intervals of increased aridity are documented, and they are interrupted by two relatively humid stages. The three relatively arid intervals are 6.865~6.378 Ma, 5.583~4.4 Ma and 3.62~2 Ma, and the two relative humid periods occurred at 6.378~5.583 Ma and 4.4~3.62 Ma.

Regional precipitation variations, recorded by mineral assemblages during the period of the late Miocene to early Pleistocene, are linked to the migration of the westerlies, which provides a feedback for global cooling.

The evolution of the westerlies during the late Miocene and early Pleistocene was driven by global cooling, which caused the path of the westerly winds to be displaced southward, and as a consequence less moisture reached the Tarim Basin. This was the primary reason for the aridification of the Asian interior since the late Miocene. Tectonic uplift of the Tibetan Plateau likely contributed as a secondary factor.

**Supplementary Materials:** The following supporting information can be downloaded at: <https://www.mdpi.com/article/10.3390/min12121543/s1>, Table S1: Data set of mineral concentration for the drilling core LS2 from the Tarim Basin.

**Author Contributions:** Resources, X.Q. and W.L.; writing—original draft preparation, M.Y.; writing—review and editing, H.C. and G.S.B. All authors have read and agreed to the published version of the manuscript.

**Funding:** This research received no external funding.

**Data Availability Statement:** The authors confirm that the data supporting the findings of this study are available within the supplementary materials.

**Acknowledgments:** This research was jointly supported by the Second Tibetan Plateau Scientific Expedition (STEP) program (2019QZKK0707), the Strategic Priority Research Program of Chinese Academy of Sciences (XDB40010100, XDB26000000). It is a part of the “Belt and Road” project of IEECAS. We are grateful to Professors Liangcheng Tan in Institute of Earth Environment, CAS and Chaofeng Fu in Chang’an University for their hard work in field.

**Conflicts of Interest:** We declare that we do not have any commercial or associative interest that represents a conflict of interest in connection with the work submitted.

## References

1. Sun, J.; Liu, W.; Liu, Z.; Deng, T.; Windley, B.F.; Fu, B. Extreme aridification since the beginning of the Pliocene in the Tarim Basin, western China. *Palaeogeogr. Palaeoclimatol. Palaeoecol.* **2017**, *485*, 189–200. [[CrossRef](#)]
2. Tang, Z.; Yang, S.; Qiao, Q.; Yin, F.; Huang, B.; Ding, Z. A high-resolution geochemical record from the Kuche depression: Constraints on early Miocene uplift of South Tian Shan. *Palaeogeogr. Palaeoclimatol. Palaeoecol.* **2016**, *446*, 1–10. [[CrossRef](#)]
3. Zhu, B.; Yu, J.; Qin, X.; Rioual, P.; Zhang, Y.; Xiong, H. Formation and evolution of sand deserts in Xinjiang, Northwest China: II. The palaeo-environmental reconstruction. *J. Geogr. Sci.* **2014**, *24*, 539–559. [[CrossRef](#)]
4. Caves, J.K.; Winnick, M.J.; Graham, S.A.; Sjoström, D.J.; Mulch, A.; Chamberlain, C.P. Role of the westerlies in Central Asia climate over the Cenozoic. *Earth Planet. Sci. Lett.* **2015**, *428*, 33–43. [[CrossRef](#)]
5. Chang, H.; An, Z.; Wu, F.; Song, Y.; Qiang, X.; Li, L. Late Miocene-early Pleistocene climate change in the mid-latitude westerlies and their influence on Asian monsoon as constrained by the K/Al ratio record from drill core Ls2 in the Tarim Basin. *Catena* **2017**, *153*, 75–82. [[CrossRef](#)]
6. Zhang, Z.; Han, W.; Fang, X.; Song, C.; Li, X. Late Miocene-Pleistocene aridification of Asian inland revealed by geochemical records of lacustrine-fan delta sediments from the western Tarim Basin, NW China. *Palaeogeogr. Palaeoclimatol. Palaeoecol.* **2013**, *377*, 52–61. [[CrossRef](#)]
7. Liu, W.; Liu, Z.; An, Z.; Sun, J.; Chang, H.; Wang, N.; Dong, J.; Wang, H. Late Miocene episodic lakes in the arid Tarim Basin, western China. *Proc. Natl. Acad. Sci. USA* **2014**, *111*, 16292–16296. [[CrossRef](#)]
8. Zhang, Z.; Sun, J. Palynological evidence for Neogene environmental change in the foreland basin of the southern Tianshan range, northwestern China. *Glob. Planet. Chang.* **2011**, *75*, 56–66. [[CrossRef](#)]
9. Chang, H.; An, Z.; Liu, W.; Wu, F.; Qiang, X.; Song, Y. Late Miocene-early Pleistocene paleoproductivity variations of the Lop Nor in the Tarim Basin and its implications on aridification in Asian Interior. *Chin. Sci. Bull.* **2014**, *59*, 3650–3658. [[CrossRef](#)]
10. Ramstein, G.; Fluteau, F.; Besse, J.; Joussaume, S. Effect of orogeny, plate motion and land-sea distribution on Eurasian climate change over the past 30 million years. *Nature* **1997**, *386*, 788–795. [[CrossRef](#)]
11. Raymo, M.E.; Ruddiman, W.F. Tectonic forcing of late Cenozoic climate. *Nature* **1992**, *359*, 117–122. [[CrossRef](#)]
12. Gyawali, A.R.; Wang, J.; Ma, Q.; Wang, Y.; Xu, T.; Guo, Y.; Zhu, L. Paleo-environmental change since the Late Glacial inferred from lacustrine sediment in Selin Co, central Tibet. *Palaeogeogr. Palaeoclimatol. Palaeoecol.* **2019**, *516*, 101–112. [[CrossRef](#)]

13. N'nganga, A.; Ngos, S.; Ngueutchoua, G. The late Pleistocene-Holocene paleoclimate reconstruction in the Adamawa plateau (Central Cameroon) inferred from the geochemistry and mineralogy of the Lake Fonjak sediments. *J. Afr. Earth Sci.* **2019**, *150*, 23–36. [[CrossRef](#)]
14. McCormack, J.; Nehrke, G.; Jöns, N.; Immenhauser, A.; Kwiecien, O. Refining the interpretation of lacustrine carbonate isotope records: Implications of a mineralogy-specific Lake Van case study. *Chem. Geol.* **2019**, *513*, 167–183. [[CrossRef](#)]
15. Hay, R.L.; Kyser, T.K. Chemical sedimentology and paleoenvironmental history of Lake Olduvai, a Pliocene lake in northern Tanzania. *Geol. Soc. Am. Bull.* **2001**, *113*, 1505–1521. [[CrossRef](#)]
16. Lan, M.; Song, Y.; Cheng, L. Review on formation of lacustrine carbonate minerals and their paleoclimate significance. *J. Earth Sci. Environ.* **2022**, *44*, 156–170.
17. Singer, A. The paleoclimatic interpretation of clay minerals in sediments—a review. *Earth Sci. Rev.* **1984**, *21*, 251–293. [[CrossRef](#)]
18. Adam, M.H.; Jay, Q.; Guleed, A.; Douglas, B.; Scott, B.; Katharine, W.H.; Marie, G.D.L.S.; Andrew, S.C.; Lin, K.; Wang, X. Stable C, O and clumped isotope systematics and <sup>14</sup>C geochronology of carbonates from the Quaternary Chewaucan closed-basin lake system, Great Basin, USA: Implications for paleoenvironmental reconstructions using carbonates. *Geochim. Cosmochim. Acta* **2017**, *212*, 274–302.
19. David, T.W.; David, W. Precipitation of dolomite using sulphate-reducing bacteria from the Coorong Region, South Australia: Significance and implications. *Sedimentology* **2005**, *52*, 987–1008.
20. Li, M.; Sun, S.; Fang, X.; Wang, C.; Wang, Z.; Wang, H. Clay minerals and isotopes of Pleistocene lacustrine sediments from the western Qaidam Basin, NE Tibetan Plateau. *Appl. Clay Sci.* **2018**, *162*, 382–390. [[CrossRef](#)]
21. Chang, H.; An, Z.; Liu, W.; Qiang, X.; Song, Y.; Ao, H. Magnetostratigraphic and paleoenvironmental records for a Late Cenozoic sedimentary sequence drilled from Lop Nor in the eastern Tarim Basin. *Glob. Planet. Chang.* **2012**, *80–81*, 113–122. [[CrossRef](#)]
22. Zhang, C.; Li, Y.; Zhou, X.; Wang, Y. A sedimentological interpretation of the inverse correlation between saline mineral and detritals mineral in the Late Quaternary lake sediments. *J. Glaciol. Geocryol.* **2015**, *37*, 95–108.
23. Schütt, B. Holocene paleohydrology of playa lakes in northern and central Spain: A reconstruction based on the mineral composition of lacustrine sediments. *Quat. Int.* **2000**, *73–74*, 7–27. [[CrossRef](#)]
24. Olila, O.G.; Reddy, K.R. Influence of pH on Phosphorus Retention in Oxidized Lake Sediments. *Soil Sci. Soc. Am. J.* **1995**, *59*, 946–959. [[CrossRef](#)]
25. Sinha, R.; Raymahashay, B.C. Evaporite mineralogy and geochemical evolution of the Sambhar Salt Lake, Rajasthan, India. *Sediment. Geol.* **2004**, *166*, 59–71. [[CrossRef](#)]
26. You, X.; Jia, W.; Xu, F.; Liu, Y. Mineralogical characteristics of Ankerite and mechanisms of primary and secondary Origins. *Earth Sci.* **2018**, *43*, 4047–4055.
27. You, X.; Shu, S.; Zhu, J.; Li, Q.; Hu, W.; Dong, H. Microbially mediated dolomite in Cambrian stromatolites from the Tarim Basin, north-west China: Implications for the role of organic substrate on dolomite precipitation. *Terra Nova* **2013**, *25*, 387–395. [[CrossRef](#)]
28. Thompson, J.B.; Ferris, F.G. Cyanobacterial precipitation of gypsum, calcite, and magnesite from natural alkaline lake water. *Geology* **1990**, *18*, 995. [[CrossRef](#)]
29. Chang, H.; An, Z.; Wu, F.; Jin, Z.; Liu, W.; Song, Y. A Rb/Sr record of the weathering response to environmental changes in westerly winds across the Tarim Basin in the late Miocene to the early Pleistocene. *Palaeogeogr. Palaeoclimatol. Palaeoecol.* **2013**, *386*, 364–373. [[CrossRef](#)]
30. Vasconcelos, C.M.; Judith, A.; Bernasconi, S.; Grujic, D.; Tiens, A.J. Microbial mediation as a possible mechanism for natural dolomite formation at low temperatures. *Nature* **1995**, *377*, 220–222. [[CrossRef](#)]
31. Quigley, R.M.; Martin, R.T. Chloritized weathering products of a New England glacial till. *Clays Clay Miner.* **1961**, *10*, 107–116. [[CrossRef](#)]
32. Fang, X.; Li, M.; Wang, Z.; Wang, J.; Li, J.; Liu, X.; Zan, J. Oscillation of mineral compositions in Core SG-1b, western Qaidam Basin, NE Tibetan Plateau. *Sci. Rep.* **2016**, *6*, 32848. [[CrossRef](#)]
33. Lybrand, R.; Rasmussen, C.; Jardine, A.; Troch, P.; Chorover, J. The effects of climate and landscape position on chemical denudation and mineral transformation in the Santa Catalina mountain critical zone observatory. *Appl. Geochem.* **2011**, *26*, S80–S84. [[CrossRef](#)]
34. Wang, C.; Hong, H.; Li, Z.; Yin, K.; Xie, J.; Liang, G.; Song, B.; Song, E.P.; Zhang, K. The Eocene-Oligocene climate transition in the Tarim Basin, Northwest China: Evidence from clay mineralogy. *Appl. Clay Sci.* **2013**, *74*, 10–19. [[CrossRef](#)]
35. Toshimura, T. Neofomation and transformation of clay minerals in diagenetic process and their characteristic features. *Nendo Kagaku* **1985**, *25*, 107–112.
36. Singer, A.; Stoffers, P. Clay mineral diagenesis in two East African lake sediments. *Clay Miner.* **1980**, *15*, 291–307. [[CrossRef](#)]
37. Tian, J.; Chen, Z.; Fan, Y.; Li, P.; Song, L. The occurrence, growth mechanism and distribution of authigenic chlorite in sandstone. *Bull. Mineral. Petrol. Geochem.* **2008**, *27*, 201–205.
38. Rao, Q.; Dai, C.; Zhang, H.; Pan, Z.; Cao, S. Occurrence and origin of chlorite in sedimentary, igneous and metamorphic rocks. *Acta Geol. Sichuan* **2016**, *36*, 561–566.
39. Yin, K.; Hong, H.; Algeo, T.J.; Churchman, G.J.; Li, Z.; Zhu, Z.; Fang, Q.; Zhao, L.; Wang, C.; Ji, K.; et al. Fe-oxide mineralogy of the Jiujiang red earth sediments and implications for Quaternary climate change, southern China. *Sci. Rep.* **2018**, *8*, 3610. [[CrossRef](#)]
40. Hui, Z.; Li, J.; Xu, Q.; Song, C.; Zhang, J.; Wu, F.; Zhao, Z. Miocene vegetation and climatic changes reconstructed from a sporopollen record of the Tianshui Basin, NE Tibetan Plateau. *Palaeogeogr. Palaeoclimatol. Palaeoecol.* **2011**, *308*, 373–382. [[CrossRef](#)]

41. Dittrich, M.; Obst, M. Are Picoplankton Responsible for Calcite Precipitation in Lakes? *Ambio* **2004**, *33*, 559–564. [[CrossRef](#)] [[PubMed](#)]
42. Sun, J.; Zhang, L.; Deng, C.; Zhu, R. Evidence for enhanced aridity in the Tarim Basin of China since 5.3 Ma. *Quat. Sci. Rev.* **2009**, *27*, 1012–1023. [[CrossRef](#)]
43. Sun, J.; Gong, Z.; Tian, Z.; Jia, Y.; Windley, B. Late Miocene stepwise aridification in the Asian interior and the interplay between tectonics and climate. *Palaeogeogr. Palaeoclimatol. Palaeoecol.* **2015**, *421*, 48–59. [[CrossRef](#)]
44. Sun, D.; Bloemendal, J.; Yi, Z.; Zhu, Y.; Wang, X.; Zhang, Y.; Li, Z.; Wang, F.; Han, F.; Zhang, Y. Palaeomagnetic and palaeoenvironmental study of two parallel sections of late Cenozoic strata in the central Taklimakan Desert: Implications for the desertification of the Tarim Basin. *Palaeogeogr. Palaeoclimatol. Palaeoecol.* **2011**, *300*, 1–10. [[CrossRef](#)]
45. Zheng, H.; Chen, H.; Cao, J. Palaeoenvironmental implication of the Plio-Pleistocene loess deposits in southern Tarim Basin. *Chin. Sci. Bull.* **2002**, *47*, 700–704. [[CrossRef](#)]
46. Fang, X.; An, Z.; Clemens, S.C.; Zan, J.; Shi, Z.; Yang, S.; Han, W. The 3.6-Ma aridity and westerlies history over midlatitude Asia linked with global climatic cooling. *Proc. Natl. Acad. Sci. USA* **2020**, *117*, 24729–24734. [[CrossRef](#)]
47. Wang, X.; Sun, D.H.; Wang, F.; Li, B.F.; Wu, S.; Guo, F.; Li, Z.J.; Zhang, Y.B.; Chen, F.H. A high-resolution multi-proxy record of late Cenozoic environment change from central Taklimakan Desert, China. *Clim. Past* **2013**, *9*, 2731–2739. [[CrossRef](#)]
48. Wu, F.; Fang, X.; Herrmann, M.; Mosbrugger, V.; Miao, Y. Extended drought in the interior of Central Asia since the Pliocene reconstructed from sporopollen records. *Glob. Planet. Chang.* **2011**, *76*, 16–21. [[CrossRef](#)]
49. Sun, Y.; An, Z. History and variability of asian interior aridity recorded by eolian flux in the chinese loess plateau during the past 7 Ma. *Sci. China Earth Sci.* **2002**, *45*, 421–429. [[CrossRef](#)]
50. Tang, Z.; Ding, Z.; White, P.D.; Dong, X.; Ji, J.; Jiang, H.; Luo, P.; Wang, X. Late Cenozoic central Asian drying inferred from a palynological record from the northern Tian Shan. *Earth Planet. Sci. Lett.* **2011**, *302*, 439–447. [[CrossRef](#)]
51. Zachos, J.; Pagani, M.; Sloan, L.; Thomas, E.; Billups, K. Trends, Rhythms, and Aberrations in Global Climate 65 Ma to Present. *Paleoclimate* **2001**, *292*, 686–693. [[CrossRef](#)] [[PubMed](#)]
52. Zheng, H. Late Miocene and mid-Pliocene enhancement of the East Asian monsoon as viewed from the land and sea. *Glob. Planet. Chang.* **2004**, *41*, 147–155. [[CrossRef](#)]
53. Miao, Y.; Herrmann, M.; Wu, F.; Yan, X.; Yang, S. What controlled Mid-Late Miocene long-term aridification in Central Asia?—Global cooling or Tibetan Plateau uplift: A review. *Earth Sci. Rev.* **2012**, *112*, 155–172. [[CrossRef](#)]
54. Nielsen, T.; Kuijpers, A. Only 5 southern Greenland shelf edgeglaciations since the early Pliocene. *Sci. Rep.* **2013**, *3*, 1875. [[CrossRef](#)] [[PubMed](#)]
55. Sun, J.; Lü, T.; Gong, Y.; Liu, W.; Wang, X.; Gong, Z. Effect of aridification on carbon isotopic variation and ecologic evolution at 5.3 Ma in the Asian interior. *Earth Planet. Sci. Lett.* **2013**, *380*, 1–11. [[CrossRef](#)]
56. Porter, S.C.; An, Z. Correlation between climate events in the North Atlantic and China during the last glaciation. *Lett. Nat.* **1995**, *375*, 305–308. [[CrossRef](#)]
57. Kudless, K.E. *Late Cenozoic Ice-rafted Debris Studies of the Southeast Greenland Margin and the North Pacific Ocean*; The Ohio State University: Genoa, Italy, 1998.
58. Alan, M.H.; Paul, J.V.; Bruce, W.S. Global scale palaeoclimate reconstruction of the middle Pliocene climate using the UKMO GCM: Initial results. *Glob. Planet. Chang.* **2000**, *25*, 239–256.
59. Ballantyne, A.P.; Greenwood, D.R.; Sinninghe Damsté, J.S.; Csank, A.Z.; Eberle, J.J.; Rybczynski, N. Significantly warmer Arctic surface temperatures during the Pliocene indicated by multiple independent proxies. *Geology* **2010**, *38*, 603–606. [[CrossRef](#)]
60. Brierley, C.M.; Fedorov, A.V. Relative importance of meridional and zonal sea surface temperature gradients for the onset of the ice ages and Pliocene-Pleistocene climate evolution. *Paleoceanography* **2010**, *25*, PA2214. [[CrossRef](#)]
61. Pan, Y.; Li, D.; Guo, F.; He, Z.; Pei, J.; Liu, J.; Zhao, Y. Geomorphological features of the Keriya River valley and the early-middle Pleistocene great lake environment of the Tarim basin. *Geol. Bull. China* **2008**, *27*, 814.